Fragment length influences affinity for Cu 2+ and Ni 2+ binding to His 96 or His 111 of the prion protein and spectroscopic evidence for a multiple histidine binding only at low pH

Mark Klewpatinond, John H Viles

12th Feb 2007

Submission to: Biochemical Journal

Fragment length influences affinity for Copper^{2+} and Nickel^{2+} binding to His^{96} or His^{111} of the prion protein and spectroscopic evidence for a multiple His binding only at low pH

Mark Klewpatinond and John H. Viles*

*Corresponding Author:
School of Biological and Chemical Sciences, Queen Mary, University of London
Mile End Road, London E1 4NS, UK
j.viles@qmul.ac.uk
Tel: (44) 020 7882 3054
Fax: (44) 020 8983 0973

Running title: Cu^{2+} binding to the Prion Protein

Abbreviations: BSE, bovine spongiform encephalopathy; CD, Circular Dichroism; CJD, Creutzfeldt-Jacob disease; GPI, glycosyl-phosphatidylinositol; PrP, prion protein; PrP^{Sc}, scrapie isoform of PrP; PrP^{C}, cellular isoform of PrP; NMR, Nuclear Magnetic Resonance; TOCSY, Total Correlation Spectroscopy; ROESY, Rotating-frame Overhauser enhancement spectroscopy.

Biochemical Journal Immediate Publication. Published on 2 Mar 2007 as manuscript BJ20061893

ABSTRACT

The prion protein (PrP) is a Cu^{2+} binding cell-surface glycoprotein. Using various PrP fragments and spectroscopic techniques, we show two Cu^{2+} ions bind to a region between residues 90-126. This region incorporates the neurotoxic portion of PrP, vital for prion propagation in transmissible spongiform encephalopathies. Pentapeptides, PrP(92-96) and PrP(107-111), represent the minimum motif for Cu^{2+}-binding to the PrP(90-126) fragment. Consequently, we were surprised that the appearance of the visible CD for two fragments of PrP, residues 90-126 and 91-115, are very different. We show these differences do not arise from a change in the coordination geometry within the two fragments, rather, there is a change in the relative preference for the two binding sites centred at His111 and His96. These preferences are metal, pH and chain-length dependent. Circular dichroism indicates that Cu^{2+} initially fills the site at His111 within the PrP(90-126) fragment. The pH dependence of the Cu^{2+} coordination is studied using EPR, visible CD and absorption spectroscopy. We present evidence that at low pH (5.5) and sub-stochiometric amounts of Cu^{2+} a multiple His complex forms but at neutral pH Cu^{2+} binds to individual histidine residues. We have shown that changes in pH and levels of extra-cellular Cu^{2+} will affect coordination mode, which has implications for the affinity, folding and redox properties of Cu-PrP.

Introduction

Transmissible spongiform encephalopathies have been linked to a misfolded form of the prion protein, PrP^{Sc}. These proteinaceous infectious particles are devoid of genetic material and represent a wholly novel infectious agent [1-3]. Normal cellular prion protein (PrP^{C}) is a cell surface glycoprotein, approximately 209 amino acids long, with a glycosylphosphatidyl inositol (GPI) anchor. PrP^{C} contains two distinct structural regions, including the unstructured N-terminal domain between residues 23-126 [4], and the mainly α-helical C-terminal domain between residues 126-231 [5]. In the absence of copper, the N-terminal domain exhibits a high degree of flexibility in the main-chain [6]. A four octarepeats sequence, PHGGGWGQ, found between residues 60-91 in the unstructured region of PrP, binds up to four Cu^{2+} ions [7-11].

One feature of prion disease is metal imbalance [12]. PrP^{Sc} has been found to be occupied with metal when isolated from diseased brain [13], whilst metal binding to the prion protein is altered in human prion disease [14]. The levels of cellular copper seems to be affected by scrapie infection [15] and copper catalysed redox damage of PrP [16] is linked to prion disease [17, 18]. Forthermore, disease progression in infected mice can be slowed with the use of copper-specific chelation therapy [19].

A direct link between copper binding to the octarepeats and prion disease has been thought unlikely, as studies of mice expressing a truncated version of PrP with the octarepeat region removed were still susceptible to prion infection [20]. However, it has been noted that Cu^{2+} ions bind outside this octarepeat region [11, 21-25]. We have shown that Cu^{2+} binds to residues His96 and His111 [21, 26], in a region considered to be essential for amyloid formation and infectivity in prion disease [27-30]. Using ^{1}H NMR and visible CD spectroscopy, we have shown that like Cu^{2+}, two Ni^{2+} ions bind to His96 and His111 independently of each other [26]. Cu^{2+} has been implicated with the toxicity of a fragment from this unstructured region, PrP(106-126), which is neurotoxic in both the soluble and fibrillar states [30-32]. Furthermore, we have shown that Cu^{2+} binding to His96 and His111 promotes the formation of β-sheet [21], which is consistent with the findings that this unstructured region is key to the misfolding of PrP^{C} into the β-sheet rich conformation [33]. Cu^{2+} can also convert the cellular prion protein into a protease-resistant species [34], which is a feature of PrP^{Sc}. The presence, or absence, of Cu^{2+} ions may also confer different strains of prion disease [13, 35].

Although the normal physiological role of PrP has yet to be determined, it may have a function in copper homeostasis due to the ability of PrP^C to bind Cu^{2+} *in vivo* and *in* vitro [7, 11]. Copper has been shown to promote the endocytosis of PrP^C [36, 37], however PrP expression levels do not seem to affect copper delivery [38, 39]. PrP^C can act as an antioxidant by sacrificially quenching hydroxyl radicals produced via Cu^{2+}/Cu^+ Fenton's cycling [16] and copper-induced cleavage of the PrP^C main-chain has been reported [40, 41].

We have previously published data of Cu^{2+} and Ni^{2+} binding to a fragment of PrP, residues 91-115 [21, 26]. In these studies we showed that both Cu^{2+} and Ni^{2+} bind to His96 and His111 independently of each other, forming a square-planar/tetragonal complex. The metal complex involves coordination of main-chain amides preceding the His imidazole, as well as the imidazole nitrogen εN. Here we present data for the larger fragment, PrP(90-126), this peptide includes additional hydrophobic residues which incorporates the neurotoxic peptide, PrP(106-126) [30-32]. This region is essential for prion propagation [27-30]. At first observation the Cu^{2+}-visible CD data for Cu_1PrP(90-126) appear to be very different from that of the slightly shorter fragment, Cu_1PrP(91-115). One of the aims of this study is to understand the reasons for the differences in the visible CD spectra. We have used a range of peptide fragments and spectroscopic techniques to characterise Cu^{2+} and Ni^{2+} binding to the amyloidogenic fragment of PrP essential for prion replication over a range of pH values and metal stoichiometries.

EXPERIMENTAL PROCEDURES

Peptide Synthesis and Purification: F-moc chemistry was used to synthesise various fragments of PrP, which were N-terminally acetylated and C-terminally amidated in order to mimic this region of PrP within the full-length protein (A.B.C., Imperial College, London). The peptides were removed from the resin and de-protected before purification by reverse-phase HPLC. The samples were characterised using mass spectrometry and ^{1}H NMR spectroscopy.

Peptide Design: Acetylated and amidated peptides included:

PrP(90-126): GQGGGT**H**SQWNKPSKPKTNMK**H**MAGAAAAGAVVGGLG

PrP(91-115): QGGGT**H**SQWNKPSKPKTNMK**H**MAGA

PrP(90-126)H111A: GQGGGT**H**SQWNKPSKPKTNMK**A**MAGAAAAGAVVGGLG

PrP(90-126)H96A: GQGGGT**A**SQWNKPSKPKTNMK**H**MAGAAAAGAVVGGLG

PrP(91-115)H111A: QGGGT**H**SQWNKPSKPKTNMK**A**MAGA

PrP(91-115)H96A: QGGGT**A**SQWNKPSKPKTNMK**H**MAGA

PrP(92-96): GGGT**H**; PrP(107-111): TNMK**H**; PrP(110-115): K**H**MAGA

Note that H96A peptides only contain His111, while H111A peptides only contain His96

Titrations: Small aliquots of fresh aqueous solutions were used to add metal ions (Cu^{2+} as $CuCl_2.2H_2O$, Ni^{2+} as $NiCl_2.6H_2O$). Peptide concentrations were determined using an extinction coefficient at 280 nm; 5690 $M^{-1}cm^{-1}$ multiplied by the number of Trp residues in the peptide [42]. In the case of peptides which lacked aromatic residues, the weight was used to approximate the concentration and a 20 % water content was assumed. All titrations were carried out in the absence of buffers and the pH was measured before and after acquiring each spectrum, adjusting the pH when necessary using small aliquots of 100 mM NaOH or HCl.

Circular Dichroism (CD): CD spectra were recorded on an Applied Photophysics Chirascan instrument at 25° C, as previously described [8]. A cell with a 1 cm pathlength was used for spectra recorded between 300 and 800 nm, with sampling points every 2 nm. Typically, four scans were recorded, and baseline spectra were subtracted from each spectrum. Data were processed using Applied Photophysics Chirascan Viewer, Microsoft Excel and the KaleidaGraph spreadsheet / graph package. The direct CD measurements (θ, in millidegrees) were converted to

molar ellipticity, $\Delta\varepsilon$ ($M^{-1}cm^{-1}$), using the relationship $\Delta\varepsilon = \theta/33{,}000 \cdot c \cdot l$, where c is the concentration and l is the pathlength.

Electron Paramagnetic Resonance Spectroscopy (EPR): X-band EPR spectra were acquired on a Bruker Elexsys E500 spectrometer operating at a microwave frequency of 9.33 GHz. The spectra were acquired over a sweep width of 2500 gauss, a modulation frequency of 10 gauss, and a temperature of ~20 K. At least two scans were acquired per sample.

Proton Nuclear Magnetic Resonance (NMR): ^{1}H NMR spectra were acquired at 296 K on a Varian Unity 600 MHz spectrometer using 5 mm inverse-detection (^{1}H), triple resonance, z-gradient probes. Spectra were recorded in 100 % D_2O, a low power pre-saturation pulse was used to suppress residual water. TOCSY spectra were typically acquired with 2048[F2] x 512[F1] complex points, employing a DIPSI2 sequence for isotropic mixing, with a mixing time of ~60 ms. The States-TPPI method was used for quadrature detection in the indirect dimension for 2D spectra. Prior to Fourier transformation, sine-squared window functions, phase shifted by 90^{o}, were applied to both dimensions and zero filled to 2048 real points. Data were processed and analysed using Vnmr (Varian) software running on a SGI O2. Proton resonance assignments of each pentapeptide were obtained using the 2D TOCSY data.

RESULTS

Visible CD of $Cu^{2+}$and Ni^{2+} binding to PrP fragments containing a single His at positions 96 and 111: Figure 1 is a comparison of the visible CD spectra of a single mole equivalent of Cu^{2+} ions bound to PrP(91-115) and the longer fragment, PrP(90-126), at pH 7.8. Initially, we were surprised at the very different appearance of the two spectra as we believe the pentapeptides, PrP(92-96) and PrP(107-111), represent the isolated Cu^{2+} binding sites and the Cu^{2+} complex should be unaffected by the presence of residues outside this region. For this reason, we set about comparing the Cu^{2+}- or Ni^{2+}-loaded visible CD spectra for the PrP(90-126) analogues containing a single His at position 96 or 111 with similar shorter PrP(91-115) fragments, and their respective pentapeptides containing His96 or His111. Figure 2(a) shows the Cu^{2+}-bound spectra (1 mole equivalent) for PrP(90-126)H111A, PrP(91-115)H111A and PrP(92-96) at pH 7.8. The three peptides show clear similarities, with a positive CD band at ~500 nm and a negative band at ~600 nm. Similarly, Figure 2(b) compares the same three peptides, but with Ni^{2+} bound (1 mole equivalent) at pH 9.0. Again, there is a positive CD band to shorter wavelengths at ~420 nm and a negative band to longer wavelengths at ~500 nm. There is little variation in the maximal position of the CD bands for both the Cu^{2+} and Ni^{2+} complex for the 3 peptide analogues, but there is some variation in the intensity. For example, in Figure 2(b), the intensities of the bands at 500 nm for Ni_1PrP(91-115)H111A, Ni_1PrP(92-96) and Ni_1PrP(90-126)H111A are -1.96 $M^{-1}cm^{-1}$, 2.38 $M^{-1}cm^{-1}$ and 3.28 $M^{-1}cm^{-1}$, respectively, i.e. 2.54 $M^{-1}cm^{-1}$ +/- 26 %. At pH ~7.8, the position of the CD bands are relatively insensitive to pH, but the intensities are affected. However, the variations in intensity of the bands between the various fragments (+/- 26 % average intensity) may well be attributed to small variations in pH and concentration. The position of the CD bands is unaffected by fragment length, but there may be subtle effects on the intensity of the CD bands between fragments; this is supported by variations in the appearance of visible CD spectra for Cu_2(91-115) and Cu_2(90-126) (see Supplemental Figure 1).

The Cu^{2+}-bound spectra for the other metal ion binding site at His111 are compared in Figure 2(c). The PrP(90-126)H96A, PrP(91-115)H96A and PrP(107-111) spectra with 1 mole equivalent of Cu^{2+} also give very similar CD spectra, with a negative band at ~500 nm and a positive band at ~620 nm. As with the His96 containing peptides, the visible CD spectra of Ni^{2+}-

bound peptides incorporating the His111 binding site echo the Cu^{2+} binding, with a negative CD band at shorter wavelengths, 420 nm, and a positive band to longer wavelengths, 500 nm.

The visible absorption bands associated with d-d electronic transitions have the absorption maximum at ~580 nm at pH 7 (~540 nm at pH 9) for the Cu^{2+} complex with PrP(90-126) and ~440 nm for the Ni^{2+} complex at pH 8.5, as previously described [26]. There is little difference between the visible absorption bands of Cu^{2+} (or Ni^{2+}) binding at His96 compared with that of His111. The observed extinction coefficients and wavelength maxima for Cu^{2+} pH 8 $\varepsilon_{540\ nm} = 110\ M^{-1}cm^{-1}$ and Ni^{2+} pH 8.5 $\varepsilon_{440\ nm} = 140\ M^{-1}cm^{-1}$ are typical for a square-planar arrangement of nitrogen and oxygen ligands (Cu-3N1O 580 nm, Cu-4N 540 nm) for both the Cu^{2+} and Ni^{2+} complex, respectively [43].

It is interesting to note that the CD bands for both the Ni^{2+} and Cu^{2+} complexes incorporating His96 are positive to shorter wavelengths of the absorption maximum (~540 nm for Cu^{2+} and ~440 nm for Ni^{2+}) and negative to longer wavelengths. The maximal position of the CD bands do not correspond to the absorption maxima, as the absorption band is derived from three overlapping d-d transitions [44]. In contrast the CD bands for both Cu^{2+} and Ni^{2+} complexes at His111 produce negative CD bands to shorter wavelengths and positive to longer wavelengths. Thus, the complexes at His96 and His111 give CD spectra that are almost mirror images of each other. We are presently developing a rationale for the striking differences in visible CD spectra and hope to propose some empirical rules for predicting the appearance of Cu^{2+} and Ni^{2+} square-planar complexes involving His sidechain and amide main-chain coordination. In summary, the spectra in Figure 2 indicate that the two pentapeptides contain all the residues necessary to form the complex at His96 or His111. The nature of the two complexes does not appear to be influenced by additional residues present in the 91-115 or 90-126 peptide fragments.

Visible CD of PrP(90-126): Cu^{2+}: Now we have established the appearance of the visible CD spectra for PrP fragments contain a single His at position 96 or 111, we can compare these spectra to those of PrP(90-126) and PrP(91-115) in which both Histidines are present. These comparisons are to determine if the Cu^{2+} and Ni^{2+} complexes formed are isolated from each other at the two His sites, or whether a single metal ion will bind to both His96 and His111 simultaneously. Figure 3(a) shows visible CD data with 1 and 2 mole equivalents of Cu^{2+} loaded

on to PrP(90-126) at pH 7.8, similar spectra are observed at pH 9.0 (shown in supplemental material). Figure 3(c) presents simulated data created by combining CD spectra of the two analogues, PrP(90-126)H111A and PrP(90-126)H96A, each loaded with 1 mole equivalent of Cu^{2+} at various percentage ratios.

When the spectra for the one mole equivalent Cu^{2+}-bound PrP(90-126) analogues are added together (H111A + H96A), they overlay almost identically with the 2 Cu^{2+}-bound PrP(90-126) spectra, suggesting Cu^{2+} ions bind independently to either His96 or His111. The spectra of one mole equivalent of Cu^{2+} bound to PrP(90-126) look very different - the simulations show that when only 1 mole equivalent of Cu^{2+} is added to PrP(90-126) the appearance of the spectra is most readily simulated using a 0.95 : 0.05 ratio of H96A : H111A (Note H96A contains His111 only). Similar behaviour is observed at pH 9.0, shown as supplementary material. Based on these simulations, we can therefore conclude that the majority of the Cu^{2+} binds to the site at His111 within the PrP(90-126) fragment at 1 mole equivalent of Cu^{2+}.

It is now clear that as previously shown for PrP(91-115) [26], PrP(90-126) binds both Cu^{2+} ions at individual His residues. The reason for the difference in the appearance of the spectra (Figure 1) is not in fact a change in coordination geometry for the two peptides, but rather a change in the relative affinity for Cu^{2+} binding to His96 or His111. We have previously shown [26] that Cu_1PrP(91-115) can be very closely simulated by the addition of His96Ala : His111Ala at 0.72 : 0.28 ratios (shown in supplemental material). This suggests that the addition of the hydrophobic tail of 11 residues results in the metal-binding site at His111 exhibiting a higher affinity for Cu^{2+} relative to His96 rather than a change in coordination geometry. We have summarised the changes in the relative affinity for the two binding sites as shown in the presence of 1 mole equivalent of Cu^{2+} at various pH values for both PrP(91-115) and PrP(90-126), as seen in Figure 4.

Ni^{2+}: Figure 3(b) shows visible CD data for Ni^{2+} at 1 and 2 mole equivalents added onto PrP(90-126) at pH 9.0. Also shown in Figure 3(d) are Ni^{2+} loaded mixtures of PrP(90-126)H111A and PrP(90-126)H96A, simulated by the addition of the two spectra at various percentage ratios, at pH 9.0. When the analogues are added together (50 : 50) they overlay almost identically with the 2 Ni^{2+}-bound wild-type spectrum. To effectively simulate the spectrum for 1 mole equivalent of Ni^{2+} in PrP(90-126), it is clear quite different ratios of H96A and H111A are required. In the

case of Ni^{2+}, 30 % H96A and 70 % H111A produces the closest simulation. This implies that Ni^{2+} has a preference to bind to the His96 site rather than His111. The preference for metal ion binding at His111 or His96 is quite subtle, as Cu^{2+} has a preference for His111 and Ni^{2+} has a slight preference for His96 in the PrP(90-126) fragment (see Figure 4).

CW-EPR of PrP(90-126) and its analogues and pentapeptides: X-band EPR was used to investigate the ligands involved in the coordination geometry of the Cu^{2+} PrP complexes. EPR spectra of PrP(90-126) bound to 1 mole equivalent of Cu^{2+} between pH 5.5 and 9 are shown in Figure 5(a). Comparison of PrP(90-126) and PrP(91-115), as might be expected, reveal very similar spectra with similar pH dependence (data not shown). The spectra are consistent with a Type II axial geometry, suggesting a square-planar/tetragonal arrangement. At pH 6.0, a set of signals with $A_{\|}$ and $g_{\|}$ values of 15.3 mK and 2.29 are present (component 2). A Peisach-Blumberg plot [45] of these values suggests an equatorial coordination of 3N1O (or 2N2O). As the pH is raised, the $g_{\|}$ and hyperfine splittings shift slightly. At pH 8.0 and 9.0, the $A_{\|}$ and $g_{\|}$ values of 16.5 mK and 2.27 are observed, suggesting a ~ 4N (or 3N1O) coordination of the Cu^{2+} ion (component 1). The differences in the $A_{\|}$ and $g_{\|}$ values between components 1 and 2 are not sufficient that two sets of signals are resolved - there is simply a shift to higher field of the signals as the pH is raised. These two components represent a change in coordinating ligands of Cu^{2+} bound to a single His residue at His96 or His111. The two most probable complexes are indicated in Figure 6. The Cu-PrP(90-126) EPR spectrum obtained at pH 5.5 has $A_{\|}$ and $g_{\|}$ of 13.4 mK and 2.35, typical of a Type-II 2N2O complex. At this low pH, amide deprotonation even in the presence of Cu^{2+} is unfavourable and the carboxylate coordination is favoured.

EPR of peptides containing a single histidine, PrP(90-126)H111A and PrP(90-126)H96A, give similar spectra, Fig 5B. There is a shoulder on the hyperfine splitting to high field, which is more apparent in the H111A spectra. At present we have not assigned this feature. As with the visible CD spectra (Figure 3), the EPR spectra at pH 6.0 and above for the Cu^{2+} loaded PrP(90-126) fragments are readily simulated by the addition of H96A and H111A spectra as shown in Figure 5(b).

Interestingly however, it is not possible to simulate the 2N2O spectra at pH 5.5 of PrP(90-126) using PrP(90-126)H96A and PrP(90-126)H111A EPR spectra. The $A_{\|}$ and $g_{\|}$ of H96A spectra at pH 5.5 are more typical of a 4O spectra than the 2N2O spectra observed for

PrP(90-126) at the same pH. This suggests that the pH 5.5 complex may well contain the two His residues coordinating a single Cu^{2+} ion shown as component 3 in Figure 6.

The EPR spectra of the two pentapeptides were also obtained, the spectra of the two peptides are strikingly similar; both have Type-II axial geometry. At pH 7.8 and 9, the $A_{||}$ and $g_{||}$ values are very similar to that of component 1 (the 4N species), with $A_{||}$ and $g_{||}$ values of 16.5 mK and 2.27. At pH 6 the $g_{||}$ value shifts to higher field and the hyper-fine splitting reduces, with $A_{||}$ and $g_{||}$ values of 15.3 mK and 2.29, component 2 (the 3N1O species).

Finally, the possibility of a coupled Cu^{2+} system with a single bridged His was investigated. The spectra are not affected by increases in temperature from 20 K to 120 K, which suggests that copper is not coupled and there is no Histidine bridging between the two Cu^{2+} ions.

pH dependence of binding: To complement the pH dependence studies by EPR, Figure 7 shows the pH dependence of the visible CD spectra of the two pentapeptides, PrP(107-111) and PrP(92-96). There is a clear transition in the spectra at ~pH 7. Although, at pH 7.8 and above the two pentapeptides give the characteristic mirror-images of each other. We note that at pH 6.0 the spectra of the two pentapeptides have a good deal of similarity, with both peptides giving a weaker positive CD band at ~530 nm. The change in coordination mode is most apparent from the PrP(107-111) spectra, Figure 7(b). However, the PrP(92-96) spectra also change from a strong positive band at 500 nm and a negative band at 600 nm to a single weaker band at 530 nm. In agreement with the EPR data (Figure 5) The change in the spectra between pH 7.8 and 7.0 for the single His containing analogues suggests a change in coordination geometry between predominately 4N at pH 7.8 and above and a 3N1O complex at pH 7.0.

Cu^{2+} binding to multiple His residues at low pH: It is clear that at pH 7.8 and pH 9 the visible CD spectra of PrP(90-126) containing both His96 and His111 can be readily simulated using spectra of a single His-containing PrP(90-126) H96A and H111A analogue as previously described (Figure 3 and Supplementary Fig S1). It is also possible to simulate the low pH (6.5) CD spectra of PrP(90-126) from the H96A and H111A analogues, suggesting that even at low pH, single His binds to each Cu^{2+} ion as shown in Figure 8(a). We do note however, that while the spectra at pH 6.5 (and pH 6.2, Supplementary Figure S1) simulate the trend of the wild-type spectra, the spectra are not a very good fit. The positive CD signal at 530 nm is consistently

weaker in the simulated spectra for both the PrP(90-126) and PrP(91-115) fragments. A proportion of another component with a positive CD signal at ~530 nm must also be present.

We were interested in probing the effect of low stoichiometric amounts of Cu^{2+} at low pH on the mode of coordination. Figure 8(b) shows visible CD spectra of PrP(90-126) at pH 6.5 with a titration of 0.1 mole equivalent additions of Cu^{2+} ions. Plotting of a binding curve at 530 nm, is shown as an insert in Figure 8(b) and reveals a slightly sigmoidal binding curve. In particular, with 0.1 and 0.2 mole equivalent of Cu^{2+} added to PrP(90-126), the visible CD gives almost no signal. We note that the visible CD of the multiple His complex (component III, Figure 6) would produce a very weak visible CD spectra, as amide chelation which produces the vicinal effect seen in visible CD spectra is reduced or absent in this complex [46, 47]. The sigmodal curve at pH 6.5 hints at the presence of low amounts of component III with two His coordinating a single Cu^{2+} ion.

We then decided to look more closely at the visible CD and visible absorption spectra of PrP at below the stoichiometric amounts of Cu^{2+}. Figures 8(c) and (d) show visible CD and the associated absorption spectra over a range of pH values with 0.4 mole-equivalent of Cu^{2+} present. Comparison of the visible CD signal at 530 nm (Figure 8c), observed at low pH with that of a visible absorption band at 590 nm (Figure 8d) reveals some important differences in their appearance. In particular, at pH 5.5 there is no detectable visible CD, but visible absorption spectra at pH 5.5 are apparent with an $\varepsilon_{\lambda 590\ nm}$ of 35 $M^{-1}cm^{-1}$, typical of a 2N2O tetragonal complex [43]. A visible CD signal is not apparent until the pH is raised to 6.0, where a weak positive band at 530 nm is observed (assigned to a 3N1O single His complex at His96 or His111; component II). Again, at pH 5.5 a multiple His complex (component III) is suggested because the visible CD spectra of multiple His complex between pH 5.0 and 6.0 is unlikely to generate a visible CD signal, while in contrast, the visible absorption spectra is clearly observed.

^{1}H NMR studies of Ni^{2+} binding to PrP pentapeptides – measuring χ_1 coupling of His side-chain: To further investigate the nature of the metal complex at His96 and His111, ^{1}H NMR of Ni^{2+}-bound PrP fragments was undertaken. Cu^{2+}-bound PrP has square-planar geometry, but its paramagnetic properties make ^{1}H NMR spectra difficult to interpret. Therefore, Ni^{2+} was used as a probe of the Cu^{2+}-PrP complex, as Ni^{2+} often mimics Cu^{2+} binding and when in square-planar low-spin geometry, will produce a diamagnetic complex [48, 49].

^{1}H NMR studies of Ni^{2+} binding to PrP(91-115) have previously been described in detail by ourselves [26]. Ni^{2+} titration for both pentapeptides, PrP(92-96) and PrP(107-111), at pH 9 show a single complex formed in slow exchange with a 1:1 stoichiometry. Analysis of the ^{1}H NMR spectra for the two pentapeptides enabled the observation of changes in chemical shifts when Ni^{2+} is bound. Characteristic changes in chemical shift upon Ni^{2+} coordination indicate the ligands involved in coordination. In particular, αH chemical shifts of Gly94, Thr95, His96, Met109, Lys110 and His111 are the most perturbed upon Ni^{2+} coordination. The coordination shifts are characteristic of the adjacent main-chain amides being directly involved in chelating the Ni^{2+} ion in PrP(92-96) and PrP(107-111).

The predicted 4N square-planar geometry of these two divalent metal-ion binding sites at residues His96 and His111 are shown in Figure 6. Modelling these complexes, we were aware that the complex could have two different conformations and yet retain their square-planar geometry and ligands. The differences could be in the six-membered chelate ring between the His εN and His αN. The imidazole ring remains in the plane of the square-planar arrangement, but the position of the His C^{β} can be above or below the plane. This ring pucker is analogous to 'chair' and 'boat' conformations in hexane rings, and is also shown in Figure 6. We were interested in the possibility that the source of the difference in the visible CD for the binding at His111 and His96 might arise from differences in the ring pucker.

Scalar J-coupling in NMR is very sensitive to the torsion angle between coupled protons, and the H_{α}-H_{β} coupling of His96 and His111 is related to the χ_1 angle [50]. Figure 9 shows the H_{β} and $H_{\beta'}$ of the His residues for these two pentapeptides. The expected two sets of doublets of doublets are well resolved for the Ni_1PrP(107-111) complex and the ^{1}H J-coupling is readily measured from the 1D spectra, Figure 9. The αβ and αβ′ ^{3}J-couplings give values of 6.0 Hz and 7.2 Hz. J coupling ~6 Hz for both αβ and αβ′ in the Ni^{2+} bound spectra indicate a χ angle of 60° [50]. In the case of the PrP(92-96) spectrum, the H_{β} and $H_{\beta'}$ chemical shifts are almost degenerate - the two sets of doublets of doublets have coalesced into a single group of overlaid peaks upon Ni^{2+} addition, Figure 9(b). However, even from this spectrum it is clear that all J-coupling values are < 7 Hz, thus, the χ angle must also be 60° [50]. Alternative conformers (-60° and 180°) can be ruled out, as J-values of 12-14 Hz for one or other of the $^3J_{H\alpha\text{-}H\beta}$ values are required. Thus, the differences in the CD spectra (shown in Figure 2) are not due to ring

puckering, as both complexes have the same χ angle. The spectra were also acquired at 800 MHz, and the same J-coupling values were observed at the higher field strength.

DISCUSSION

Previously we have shown that Cu^{2+} and Ni^{2+} bind to both His96 and His111 independently in the PrP(91-115) fragment [26]. Pentapeptides, PrP(92-96) and PrP(107-111), contain all the residues necessary for the two binding sites. We were therefore surprised to observe very different visible CD for PrP(90-126) compared to PrP(91-115). By using H111A and H96A analogues of PrP(90-126) and PrP(91-115) containing a single His residue, we have shown that the mode of Cu^{2+} and Ni^{2+} coordination has not changed for the larger fragment. The reasons for the significant difference between the visible CD spectra of PrP(91-115) and PrP(90-126) is the relative affinity of the two sites. For example, upon the addition of one mole equivalent of Cu^{2+} to PrP(91-115) (pH 7.8), we observed ~70 % of Cu^{2+} binding to His111 and ~30 % to His96. In contrast, when the longer fragment, PrP(90-126), is used, ~95 % of Cu^{2+} binds to His111 and only 5% to His96. This has the effect of dramatically altering the appearance of the spectra.

The relative preference for His96 or His111 is interesting and varies considerably depending on the metal ion coordinating, the pH at which coordination takes place and the presence of a hydrophobic tail (residues 116-126). The complex centred at His111 has a higher affinity for Cu^{2+} than His96. The opposite might be expected as Gly94 and Gly93 main-chain coordination for the His96 complex might allow less steric strain in the complex. It appears that the hydrophobic residues increase the relative affinity of Cu^{2+} for His111. In contrast, the reverse effect is observed for the Ni^{2+} complex, as the His96 site has a slightly higher affinity. EPR does not support the presence of an axial ligand stabilising in the His111 complex, as Cu-PrP(92-96) is indistinguishable from Cu-PrP(107-111) by EPR, although this possibility is not ruled out, as axial ligands can have only subtle effects on Type-II EPR spectra.

A recent paper has suggested Cu^{2+} coordinates C-terminally from the His96 and His111 as well as N-terminally [51]. It is clear from Figure 2 and ^{1}H NMR of the Ni^{2+} complexes that removal of residues to the C-terminus of His96 or His111 for the penta-peptides do not have any substantially effect on the co-ordination. Furthermore the CD spectra with amide coordination to the N-terminus has a very different appearance as is indicated for the hexa-peptide PrP(110-106)

shown as supplemental material and for the octarepeat peptides [7, 8]. The study was based on the effect of paramagnetic broadening of the Cu^{2+} ion in ^{1}H NMR spectra [51]. The 'through-space' paramagnetic broadening to the C-terminus of the Cu^{2+} binding site could be caused by the inherent flexibility of the peptide sampling transient conformations in which these residues become close to the paramagnetic ion for brief periods of time.

The visible CD spectra of PrP(90-126)H111A and PrP(90-126)H96A analogues containing a single His residue are relatively unaffected by pH between pH ~7.5 and 9, suggesting that 4N complexes dominate at physiological pH and above. In contrast, there is a profound change in the visible CD spectra between pH ~6 and ~7.5, suggesting a change in coordinating ligands. Our EPR work also indicates that Cu^{2+} coordination is pH dependent with a probable 3N1O complex dominating at pH ~6.5 and 4N complex at pH 7.5. This agrees with a potentiometric study of PrP(92-96) and PrP(103-113) fragment which indicates the same transition from 3N1O to 4N, with the 4N dominating at above pH 7.6 [52, 53]. These two coordination modes have recently been modelled using *ab initio* electronic structure calculations [54].

The complexes, components 1 and 2 (Figure 6), require deprotonation of a number of amides. We postulate that at low pH, a multiple His complex, component 3 is favoured. The presence of a visible absorption band and EPR spectra at pH 5.5 coupled with the absence of visible CD bands at the identical pH supports this assertion. This type of complex favoured at low pH and low Cu^{2+} stoichiometry has been shown to be present in multiple octarepeats of PrP [10, 55-57]. Metal ion complexes are often described in terms of a single coordination geometry. In the case of PrP^{C}, it is more appropriate to describe the complex formed as an equilibrium between a number of complexes. The dominant species will be influenced by pH and the stoichiometric levels of Cu^{2+} ions present. The presence of a multiple His complex at sub-stoichiometric Cu^{2+} seems only to have appreciable amounts close to pH 5.5. At pH 7.4 the complex with a single histidine and amide coordination dominates. *In vivo* PrP will experience very different pHs as it is trafficked between the cell-surface and the lower pHs found in the endosome. Clearly, the pH will affect the affinity for Cu^{2+} ions for PrP and the coordination mode, which will in turn affect the Cu^{2+}-induced folding or misfolding of PrP.

Full-length PrP^{C} binds between 5 and 6 Cu^{2+} ions [11, 22]; four Cu^{2+} ions in the octarepeat region and further Cu^{2+} binding at His96/111. The N-terminal region, residues 23-

126, is unstructured in the absence of Cu^{2+}, thus, fragments of PrP from this region have been used as models for Cu^{2+} coordination to full-length PrP to circumvent solubility problems for full-length PrP at physiological pH with Cu^{2+} ions present. ESEEM-EPR studies [25] suggest that only the Cu^{2+} complex centred at His96 has an appreciable affinity with 4N square-planar coordination geometry. Alternatively, it has been proposed that His96 and His111 could coordinate a single Cu^{2+} ion [23, 24]. Our studies here have shown that Cu^{2+} binds to His111 independently of His96.

The relative preference for binding at His96 and His111 is affected by fragment length, it remains to be established if the presence of the structure C-terminal domain of PrP will affect the binding of Cu^{2+} further. Two sets of fragments can be generated *in vivo*, in addition to full-length PrP. The so-called alpha cleavage at residue 110/111 creates a metal binding fragment, 23-110, which contains the His96 binding site and the octarepeats. ROS mediated beta-cleavage occurs within, or adjacent to, the octarepeats to produce a fragment that contains both His96 and His111 but lacks most or all of the octa-repeats [41, 42]. This *in vivo* fragment created relates to our model fragment, PrP(90-126), but contains the structured C-terminal domain as well. The Cu^{2+} and Ni^{2+} coordination sites described here involve metal binding to an unstructured protein. Unlike preformed sites observed for many metallo-proteins, the main-chain must be highly flexible before ion coordination, in order that it may 'wrap' around the metal ion in a square-planar geometry. PrP^{C} is unusual in that half of it's main-chain is natively unstructured, facilitating the coordination of five to six Cu^{2+} ions.

The affinity of Cu^{2+} for PrP is still hotly debated in the literature [22, 55, 58, 59]. Two recent studies of Cu^{2+} binding to the four octarepeats fragment suggests at sub-stoichiometric amounts of Cu^{2+}, a single Cu^{2+} ion will bind to multiple His residues with a nM affinity [55, 57]. Perhaps counter-intuitively, simulations suggest that this high affinity site is out-competed by a lower affinity binding mode of four Cu^{2+} ions with μM affinity [55]. We have shown that Cu^{2+} binding to the PrP(91-115) fragment preferentially binds Cu^{2+} over the octarepeat fragment with a nM affinity [21]. Kramer has suggested a μM affinity for full-length PrP , while others have suggested femto molar affinity for the full-length protein [23, 58] when a copper-glycine chealate was used.

A role for PrP^{C} could be as a sensor of elevated Cu^{2+} levels, as Cu^{2+} levels can be as high as 0.1 mM in the synaptic cleft [60], compared to typical extra-cellular Cu^{2+} levels of 10 nM

[61]. PrP may act as a neuro-protectant during fluxes of Cu^{2+} produced at the synapse, as knockout mice are more sensitive to oxidative stress. $Copper^{2+}$ binding causes folding up of PrP, resulting in endocytosis [36, 37], however, PrP expression does not seem to significantly affect intra-cellular copper levels [38, 39].

Oxidative damage is a key feature of prion disease pathology and binding of up to six Cu^{2+} ions to PrP^C infers PrP may localise the production of radical oxygen species (ROS) via Fentons cycling of $Cu^{2+/+}$. PrP can act as a sacrificial anti-oxidant [16] resulting in chemical modification of PrP^C by ROS which could influence PrP mis-folding [17, 62]. The mode of $copper^{2+}$ coordination is influenced by Cu^{2+} stoichiometry and pH, which in turn will have a profound influence on the structuring of the N-terminal tail and biophysical properties of PrP^C. The Cu^{2+} loaded state of PrP should certainly be considered when investigating its folding and fibrillisation properties. $Copper^{2+}$ coordination causes significant loss of solubility [7] and an increased protease resistance [34]. $Copper^{2+}$ binding in the amyloidogenic region (residues 90-126) promotes β-like extended structure [21], which suggests a role for Cu^{2+} ions in promoting extended β-sheet like structures found in protofibrils. This is supported by the observation that prion disease strain type can be conferred by Cu^{2+} ions [13]. Here we have shown that the copper co-ordination mode is highly sensitive to pH, stoichiometry and PrP fragment length. This in turn will affect the affinity, redox properties and Cu^{2+} induced folding of the PrP main-chain. Thus, changes in pH or levels of Cu^{2+} ions may trigger hydroxyl radical production or amyloidogenicity of PrP observed in prion disease.

ACKNOWLEDGEMENTS: This work was funded by BBSRC Project Grants. MK is supported by a BBSRC Studentship. Our thanks to Dr Steve Rigby for EPR assistance and NIMR, Mill Hill, for use of NMR facilities. Thanks to Dr Chris Jones for useful discussions.

REFERENCES

1 Prusiner, S. B. (1997) Prion diseases and the BSE crisis. Science **278**, 245-251

2 Horwich, A. L. and Weissman, J. S. (1997) Deadly conformations--protein misfolding in prion disease. Cell **89**, 499-510

3 Prusiner, S. B. (1998) Prions. Proc. Natl. Acad.Sci. USA. **95**, 13363-13383

4 Donne, D. G., Viles, J. H., Groth, D., Mehlhorn, I., James, T. L., Cohen, F. E., Prusiner, S. B., Wright, P. E. and Dyson, J. H. (1997) Structure of the recombinant full-length hamster prion protein PrP(29-231): the N terminus is highly flexible. Proc. Natl. Acad. Sci. USA. **94**, 13452-13457

5 Riek, R., Hornemann, S., Wider, G., Billeter, M., Glockshuber, R. and Wuthrich, K. (1996) NMR structure of the mouse prion protein domain PrP(121-321). Nature **382**, 180-182

6 Viles, J. H., Donne, D., Kroon, G., Prusiner, S. B., Cohen, F. E., Dyson, H. J. and Wright, P. E. (2001) Local structural plasticity of the prion protein. Analysis of NMR relaxation dynamics. Biochemistry **40**, 2743-2753

7 Viles, J. H., Cohen, F. E., Prusiner, S. B., Goodin, D. B., Wright, P. E. and Dyson, J. H. (1999) Copper binding to the prion protein: Structural implications of four identical cooperative binding sites. Proc. Natl. Acad. Sci. USA **96**, 2042-2047

8 Garnett, A. P. and Viles, J. H. (2003) Copper binding to the octarepeats of the prion protein. Affinity, specificity, folding, and cooperativity: insights from circular dichroism. J. Biol. Chem. **278**, 6795-6802

9 Burns, C. S., Aronoff-Spencer, E., Dunham, C. M., Lario, P., Avdievich, N. I., Antholine, W. E., Olmstead, M. M., Vrielink, A., Gerfen, G. J., Peisach, J., Scott, W. G. and Millhauser, G. L. (2002) Molecular features of the copper binding sites in the octarepeat domain of the prion protein. Biochemistry **41**, 3991-4001

10 Chattopadhyay, M., Walter, E. D., Newell, D. J., Jackson, P. J., Aronoff-Spencer, E., Peisach, J., Gerfen, G. J., Bennett, B., Antholine, W. E. and Millhauser, G. L. (2005) The octarepeat domain of the prion protein binds Cu(II) with three distinct coordination modes at pH 7.4. J. Am. Chem. Soc. **127**, 12647-12656

11 Brown, D. R., Qin, K., Herms, J. W., Madlung, A., Manson, J., Strome, R., Fraser, P. E., Kruck, T., von Bohlen, A., Schulz-Schaeffer, W., Giese, A., Westaway, D. and Kretzschmar, H. (1997) The cellular prion protein binds copper in vivo. Nature **390**, 684-687

12 Thackray, A. M., Knight, R., Haswell, S. J., Bujdoso, R. and Brown, D. R. (2002) Metal imbalance and compromised antioxidant function are early changes in prion disease. Biochem. J. **362**, 253-258

13 Wadsworth, J. D. F., Hill, A. F., Joiner, S., Jackson, G. S., Clarke, A. R. and Collinge, J. (1999) Strain-specific prion-protein conformation determined by metal ions. Nat. Cell Biol. **1**, 55-59

14 Wong, B. S., Chen, S. G., Colucci, M., Xie, Z., Pan, T., Liu, T., Li, R., Gambetti, P., Sy, M. S. and Brown, D. R. (2001) Aberrant metal binding by prion protein in human prion disease. J. Neurochem. **78**, 1400-1408

15 Rachidi, W., Mange, A., Senator, A., Guiraud, P., Riondel, J., Benboubetra, M., Favier, A. and Lehmann, S. (2003) Prion infection impairs copper binding of cultured cells. J. Biol. Chem. **278**, 14595-14598

16 Nadal, R. C., Abdelraheim, S. R., Brazier, M. W., Rigby, S. E., Brown, D. R. and Viles, J. H. (2007) Prion protein does not redox-silence Cu(2+), but is a sacrificial quencher of hydroxyl radicals. Free Radic. Biol. Med. **42**, 79-89

17 Requena, J. R., Groth, D., Legname, G., Stadtman, E. R., Prusiner, S. B. and Levine, R. L. (2001) Copper-catalyzed oxidation of the recombinant SHa(29-231) prion protein. Proc. Natl. Acad. Sci. USA. **98**, 7170-7175

18 Ruiz, F. H., Silva, E. and Inestrosa, N. C. (2000) The N-terminal tandem repeat region of human prion protein reduces copper: role of tryptophan residues. Biochem. Biophys. Res. Commun. **269**, 491-495

19 Sigurdsson, E. M., Brown, D. R., Alim, M. A., Scholtzova, H., Carp, R., Meeker, H. C., Prelli, F., Frangione, B. and Wisniewski, T. (2003) Copper chelation delays the onset of prion disease. J. Biol. Chem. **278,** 46199-46202

20 Flechsig, E., Shmerling, D., Hegyi, I., Raeber, A. J., Fischer, M., Cozzio, A., von Mering, C., Aguzzi, A. and Weissmann, C. (2000) Prion protein devoid of the octapeptide repeat region restores susceptibility to scrapie in PrP knockout mice. Neuron **27**, 399-408

21 Jones, C. E., Abdelraheim, S. R., Brown, D. R. and Viles, J. H. (2004) Preferential Cu2+ Coordination by His96 and His111 Induces {beta}-Sheet Formation in the Unstructured Amyloidogenic Region of the Prion Protein. J. Biol. Chem. **279**, 32018-32027

22 Kramer, M. L., Kratzin, H. D., Schmidt, B., Romer, A., Windl, O., Liemann, S., Hornemann, S. and Kretzschmar, H. (2001) Prion protein binds copper within the physiological concentration range. J. Biol. Chem. **276**, 16711-16719

23 Jackson, G. S., Murray, I., Hosszu, L. L. P., Gibbs, N., Waltho, J. P., Clarke, A. R. and Collinge, J. (2001) Location and properties of metal-binding sites on the human prion protein. Proc. Natl. Acad. Sci. USA. **98**, 8531-8535

24 Hasnain, S. S., Murphy, L. M., Strange, R. W., Grossmann, J. G., Clarke, A. R., Jackson, G. S. and Collinge, J. (2001) XAFS study of the high-affinity copper-binding site of human PrP91-231 and its low-resolution structure in solution. J. Mol. Biol. **311**, 467-473

25 Burns, C. S., Aronoff-Spencer, E., Legname, G., Prusiner, S. B., Antholine, W. E., Gerfen, G. J., Peisach, J. and Millhauser, G. L. (2003) Copper coordination to the full-length, recombinant prion protein. Biochemistry **44**, 6794-6803

26 Jones, C. E., Klewpatinond, M., Abdelraheim, S. R., Brown, D. R. and Viles, J. H. (2005) Probing copper2+ binding to the prion protein using diamagnetic nickel2+ and 1H NMR: the unstructured N terminus facilitates the coordination of six copper2+ ions at physiological concentrations. J. Mol. Biol. **346**, 1393-407

27 Muramoto, T., Scott, M., Cohen, F. E. and Prusiner, S. B. (1996) Recombinant scrapie-like prion protein of 106 amino acids is soluble Proc. Natl. Acad. Sci. USA **93**, 15457-15462

28 Fischer, M., Rulicke, T., Raeber, A., Sailer, A., Moser, M., Oesch, B., Brandner, S., Aguzzi, A. and Weissmann, C. (1996) Prion protein (PrP) with amino-proximal deletions restoring susceptibility of PrP knockout mice to scrapie. EMBO J. **15**, 1255-64

29 Muramoto, T., DeArmond, S. J., Scott, M., Telling, G. C., Cohen, F. E. and Prusiner, S. B. (1997) Heritable disorder resembling neuronal storage disease in mice expressing prion protein with deletion of an alpha-helix. Nat. Med. **3**, 750-755

30 Brown, D. R., Schmidt, B. and Kretzschmar, H. A. (1996) Role of microglia and host prion protein in neurotoxicity of a prion protein fragment. Nature **380**, 345-347

31 Florio, T., Paludi, D., Villa, V., Principe, D. R., Corsaro, A., Millo, E., Damonte, G., A'rrigo, C., Russo, C., Schettini, G. and Aceto, A. (2003) Contribution of two conserved glycine residues to fibrillogenesis of the 106-126 prion protein fragment. Evidence that a soluble variant of the 106-126 peptide is neurotoxic. J. Neurochem. **85**, 62-72

32 Jobling, M. F., Huang, X., Stewart, L. R., Barnham, K. J., Curtain, C., Volitakis, I., Perugini, M., White, A. R., Cherny, R. A., Masters, C. L., Barrow, C. J., Collins, S. J., Bush, A. I. and Cappai, R. (2001) Copper and zinc binding modulates the aggregation and neurotoxic properties of the prion peptide PrP106-126. Biochemistry **40**, 8073-8084

33 Tagliavini, F., Prelli, F., Verga, L., Giaccone, G., Sarma, R., Gorevic, P., Ghetti, B., Passerini, F., Ghibaudi, E., Forloni, G. and et al. (1993) Synthetic peptides homologous to prion protein residues 106-147 form amyloid-like fibrils in vitro. Proc. Natl. Acad. Sci. USA **90**, 9678-9682

34 Quaglio, E., Chiesa, R. and Harris, D. A. (2001) Copper converts the cellular prion protein into a protease-resistant species that is distinct from the scrapie isoform. J. Biol. Chem. **276**, 11432-11438

35 Qin, K., Yang, D. S., Yang, Y., Chishti, M. A., Meng, L. J., Kretzschmar, H. A., Yip, C. M., Fraser, P. E. and Westaway, D. (2000) Copper(II)-induced conformational changes and protease resistance in recombinant and cellular PrP. Effect of protein age and deamidation. J. Biol. Chem. **275**, 19121-19131

36 Pauly, P. C. and Harris, D. A. (1998) Copper stimulates endocytosis of the prion protein. J. Biol. Chem. **273**, 33107-33110

37 Perera, W. S. and Hooper, N. M. (2001) Ablation of the metal ion-induced endocytosis of the prion protein by disease-associated mutation of the octarepeat region. Curr. Biol. **11**, 519-523

38 Rachidi, W., Vilette, D., Guiraud, P., Arlotto, M., Riondel, J., Laude, H., Lehmann, S. and Favier, A. (2003) Expression of prion protein increases cellular copper binding and antioxidant enzyme activities but not copper delivery. J. Biol. Chem. **278**, 9064-9072

39 Waggoner, D. J., Drisaldi, B., Bartnikas, T. B., Casareno, R. L., Prohaska, J. R., Gitlin, J. D. and Harris, D. A. (2000) Brain copper content and cuproenzyme activity do not vary with prion protein expression level. J. Biol. Chem. **275**, 7455-7458

40 Watt, N. T., Taylor, D. R., Gillott, A., Thomas, D. A., Perera, W. S. and Hooper, N. M. (2005) Reactive oxygen species-mediated beta-cleavage of the prion protein in the cellular response to oxidative stress. J. Biol. Chem. **280**, 35914-35921

41 Abdelraheim, S. R., Kralovicova, S. and Brown, D. R. (2006) Hydrogen peroxide cleavage of the prion protein generates a fragment able to initiate polymerisation of full length prion protein. Int. J. Biochem. Cell. Biol. **38**, 1429-1440

42 Gill, S. C. and von Hippel, P. H. (1989) Calculation of protein extinction coefficients from amino acid sequence data. Anal. Biochem. **182**, 319-326

43 Bryce, G. F. and Gurd, F. R. (1966) Visible spectra and optical rotatory properties of cupric ion complexes of L-histidine-containing peptides. J. Biol. Chem. **241**, 122-129

44 Martin, R. B. (1974) in Metal ions in biological systems, vol. 1 (Sigel, H., ed.), pp. 129-156, Marcel Dekker, New York

45 Peisach, J. and Blumberg, W. E. (1974) Structural implications derived from the analysis of electron paramagnetic resonance spectra of natural and artificial copper proteins. Arch. Biochem. Biophys. **165**, 691-708

46 Syme, C. D., Nadal, R. C., Rigby, S. E. and Viles, J. H. (2004) Copper binding to the amyloid-beta (Abeta) peptide associated with Alzheimer's disease: folding, coordination geometry, pH dependence, stoichiometry, and affinity of Abeta-(1-28): insights from a range of complementary spectroscopic techniques. J. Biol. Chem. **279**, 18169-18177

47 Tsangaris, J. M. and Martin, R. B. (1970) Visible circular dichroism of copper(II) complexes of amino acids and peptides. J. Am. Chem. Soc. **92**, 4255-4260

48 Laussac, J. P. and Sarkar, B. (1984) Characterization of the copper(II)- and nickel(II)-transport site of human serum albumin. Studies of copper(II) and nickel(II) binding to peptide 1-24 of human serum albumin by 13C and 1H NMR spectroscopy. Biochemistry **23**, 2832-2838

49 Sadler, P. J., Tucker, A. and Viles, J. H. (1994) Involvement of a lysine residue in the N-terminal Ni2+ and Cu2+ binding site of serum albumins. Comparison with Co2+, Cd2+ and Al3+. Eur. J. Biochem. **220**, 193-200

50 Barsukov, I. L. and Lian, L.-Y. (1993) in NMR of Macromolecules - A Practical Approach (Roberts, G. C. K., ed.), pp. 315-357, IRL Press, Oxford, UK

51 Berti, F., Gaggelli, E., Guerrini, R., Janicka, A., Kozlowski, H., Legowska, A., Miecznikowska, H., Migliorini, C., Pogni, R., Remelli, M., Rolka, K., Valensin, D. and Valensin, G. (2006) Structural and Dynamic Characterization of Copper(II) Binding of the Human Prion Protein Outside the Octarepeat Region Chemistry **13,** 1999-2001

52 Hureau, C., Charlet, L., Dorlet, P., Gonnet, F., Spadini, L., Anxolabehere-Mallart, E. and Girerd, J. J. (2006) A spectroscopic and voltammetric study of the pH-dependent Cu(II) coordination to the peptide GGGTH: relevance to the fifth Cu(II) site in the prion protein. J. Biol. Inorg. Chem. **11**, 735-744

53 Remelli, M., Donatoni, M., Guerrini, R., Janicka, A., Pretegiani, P. and Kozlowski, H. (2005) Copper-ion interaction with the 106-113 domain of the prion protein: a solution-equilibria study on model peptides. Dalton. Trans., 2876-2885

54 Cox, D. L., Pan, J. and Singh, R. R. (2006) A mechanism for copper inhibition of infectious prion conversion. Biophys. J. **91**, L11-13

55 Wells, M. A., Jelinska, C., Hosszu, L. L., Craven, C. J., Clarke, A. R., Collinge, J., Waltho, J. P. and Jackson, G. S. (2006) Multiple forms of copper(II) coordination occur throughout the disordered N-terminal region of the prion protein at pH 7.4. Biochem. J. **400**, 501-510

56 Valensin, D., Luczkowski, M., Mancini, F. M., Legowska, A., Gaggelli, E., Valensin, G., Rolka, K. and Kozlowski, H. (2004) The dimeric and tetrameric octarepeat fragments of prion protein behave differently to its monomeric unit. Dalton. Trans., 1284-1293

57 Walter, E. D., Chattopadhyay, M. and Millhauser, G. L. (2006) The affinity of copper binding to the prion protein octarepeat domain: evidence for negative cooperativity. Biochemistry **45**, 13083-13092

58 Thompsett, A. R., Abdelraheim, S. R., Daniels, M. and Brown, D. R. (2005) High affinity binding between copper and full-length prion protein identified by two different techniques. J. Biol. Chem. **280**, 42750-42758

59 Wells, M. A., Jackson, G. S., Jones, S., Hosszu, L. L., Craven, C. J., Clarke, A. R., Collinge, J. and Waltho, J. P. (2006) A reassessment of copper (II) binding in the full-length prion protein. Biochem. J. **399**, 435-444

60 Lovell, M. A., Robertson, J. D., Teesdale, W. J., Campbell, J. L. and Markesbery, W. R. (1998) Copper, iron and zinc in Alzheimer's disease senile plaques. J. Neurol. Sci. **158**, 47-52

61 Lentner, C. e. (1984) Geigy Scientific Tables Geigy Scientific Tables **3**, CIBA-GEIG Ltd., Basel, Switzerland

62 Redecke, L., Bergen, M. V., Clos, J., Konarev, P. V., Svergun, D. I., Fittschen, U. E., Broekaert, J. A., Bruns, O., Georgieva, D., Mandelkow, E., Genov, N. and Betzel, C. (2006) Structural characterization of beta-sheeted oligomers formed on the pathway of oxidative prion protein aggregation in vitro. J. Struct. Biol. **157,** 308-320

FIGURE LEGENDS

Figure 1. Comparison of visible CD spectra of $Cu_1PrP(91-115)$ and $Cu_1PrP(90-126)$ Both peptides are at pH 7.8 with 1 mole equivalent of Cu^{2+} bound to 0.1 mM peptide.

Figure 2. Visible CD spectra comparing Cu^{2+} or Ni^{2+} bound to PrP fragments containing a single Histidine at residue 96 or 111 Panels (a) and (b) compare peptides containing only His96; PrP(90-126) H111A and PrP(91-115) H111A with PrP(92-96). Panels (c) and (d) compare peptides containing only His111; PrP(90-126) H96A and PrP(91-115) H96A with PrP(107-111). Panels (a) and (c) contain 1 mole equivalent of Cu^{2+} at pH 7.8, while panels (b) and (d) contain 1 mole equivalent of Ni^{2+} at pH 9.0. All peptide concentrations were 0.1 mM.

Figure 3. Cu^{2+} and Ni^{2+} binding to PrP(90-126) and compared with simulations of H111A + H96A analogues. Panel (a) and (c) show Cu^{2+} binding and panel (b) and (d) the equivalent Ni^{2+} binding. Panel (a) shows visible CD spectra of 1 (red) and 2 (blue) mole equivalents of Cu^{2+} bound to PrP(90-126) at pH 7.8, while panel (b) shows the equivalent Ni^{2+} spectra at pH 9.0. Accompanying spectra in (c) of $Cu_1PrP(90-126)$ H111A (blue) and $Cu_1PrP(90-126)$ H96A (red) and mixtures of i, 75 : 25 %; ii, 50 : 50 %; and iii, 25 : 75 % combinations of $Cu_1PrP(90-126)$ H111A and $Cu_1PrP(90-126)$ H96A at pH 7.8. Panel (d) is the equivalent Ni^{2+} mixtures at pH 9.0. Overlaid with the spectrum of $Cu_1PrP(90-126)$ (red) is a comparable spectrum of a 95 : 5 % combination at pH 7.8 of $Cu_1PrP(90-126)$ H96A and $Cu_1PrP(90-126)$ H111A (orange). A 30 : 70 % combination at pH 9.0 is overlaid with $Ni_1PrP(90-126)$. $Cu_2PrP(90-126)$ and $Ni_2PrP(90-126)$ (blue) are similar to spectra obtained from a 1 : 1 addition (light blue) of the analogue spectra bound to 1 mole equivalent of either Cu^{2+} or Ni^{2+}. All peptide concentrations are 0.1 mM.

Figure 4. Cu^{2+} and Ni^{2+} binding preference for His96 and His111 showing pH and fragment length dependence Chart showing different percentage ratios of $Cu_1PrP(90-126)$ H111A and $Cu_1PrP(90-126)$ H96A required to simulate the spectrum of $Cu_1PrP(90-126)$ at pH 6.3, pH 7.8 and pH 9.0. The same data for PrP(91-115) is also included, as are the ratios for Ni^{2+} bound to PrP(90-126) and PrP(91-115) at pH 9.0.

Figure 5. pH dependence of Cu-PrP(90-126) EPR spectra Panel (a) is a pH titration of Cu_1PrP(90-126) and indicates the hyperfine-splitting patterns of the 3 components present. Panel (b) compares Cu_2PrP(90-126) with the simulated EPR spectrum of the addition of Cu_1PrP(90-126) H111A with Cu_1PrP(90-126) H96A at pH 7.8 (both analogue spectra are inset). Peptide concentrations of 0.1 mM, spectra were recorded at 20 K.

Figure 6. Square-planar metal binding sites at His96 and His111 in PrP(90-126) The black circle represents either a Cu^{2+} or Ni^{2+} ion. Zzz represents Thr95 or Lys110; Xxx represents Gly94 or Met109. Component 1 is a 4N complex that dominates at pH ~7.5 and above; component 2 is a 3N1O complex found at pH ~6; component 3 may form at pH 5.5 and is consistent with a 2N2O multiple His complex. The insert indicates the possible ring puckering of the C_β of the six-membered chelate ring between the histidine Nα and Nδ.

Figure 7. Visible CD spectra of pH dependence of penta-peptides (a) Cu_1PrP(92-96) and (b) Cu_1PrP(107-111). Peptide concentrations of 0.1 mM.

Figure 8. Visible CD and absorption spectra of PrP(90-126) at low pH and Cu^{2+} stoichiometry Panel (a) shows visible CD spectra of 1 (black solid line) and 2 (grey solid line) mole equivalents of Cu^{2+} bound to PrP(90-126) at pH 6.5. Overlaid with these spectra are comparable simulated spectra of a 72 : 28 % combination at pH 6.5 of Cu_1PrP(90-126) H96A and Cu_1PrP(90-126) H111A (black broken line). Cu_2PrP(90-126) is similar to spectra obtained from a 1 : 1 addition (grey broken line) of the analogue spectra bound to 1 mole equivalent of Cu^{2+}. Panel (b) is a Cu^{2+} titration of PrP(90-126) at pH 6.5, 0.1 mole equivalent additions up to 2 equivalents. Inset is a binding curve of the titration at 530 nm. Panels (c) and (d) show the pH titration of 0.4 mole equivalent Cu-PrP(90-126) by visible CD and absorption spectroscopy, respectively. Both panels show insets of their respective pH binding curves at 530 nm and 590 nm respectively. All peptide concentrations are 0.1 mM.

Figure 9. ^{1}H NMR spectra of Ni^{2+}-bound penta-petides showing His β resonances PrP(107-111) (a) and PrP(92-96) (b). The His H_β and $H_{\beta'}$ resonances are shown with J-coupling values (Hz) indicated. Peptide concentrations were 0.5 mM, 0.9 mole equivalent of Ni^{2+} at pH 9.0.

Biochemical Journal Immediate Publication. Published on 2 Mar 2007 as manuscript BJ20061893

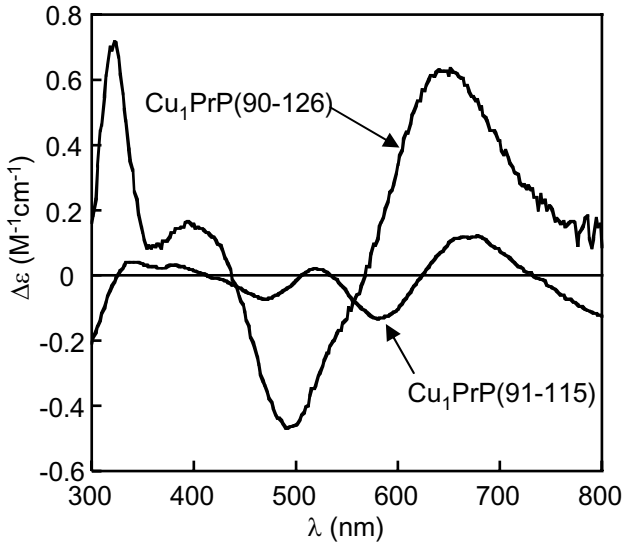

Figure 1. Klewpatinond and Viles

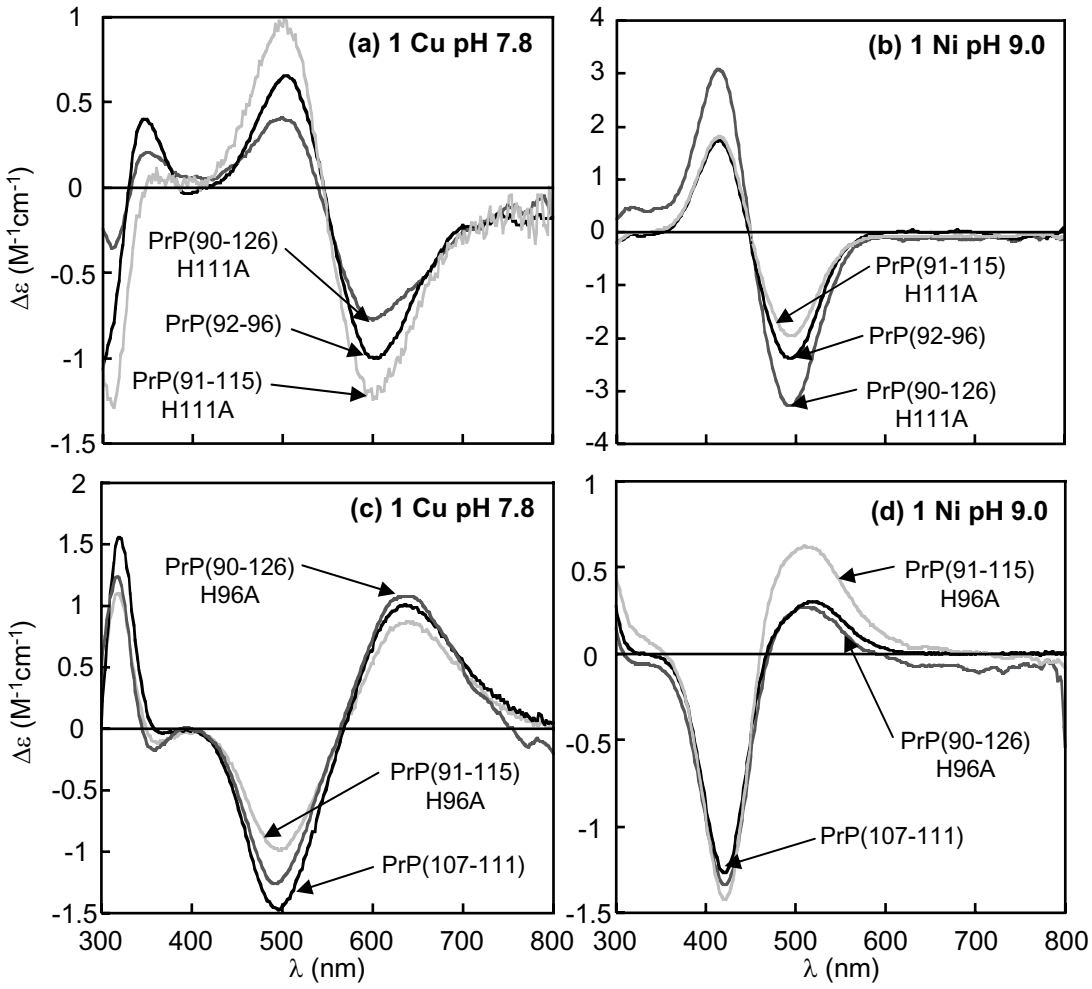

Figure 2. Klewpatinond and Viles

Biochemical Journal Immediate Publication. Published on 2 Mar 2007 as manuscript BJ20061893

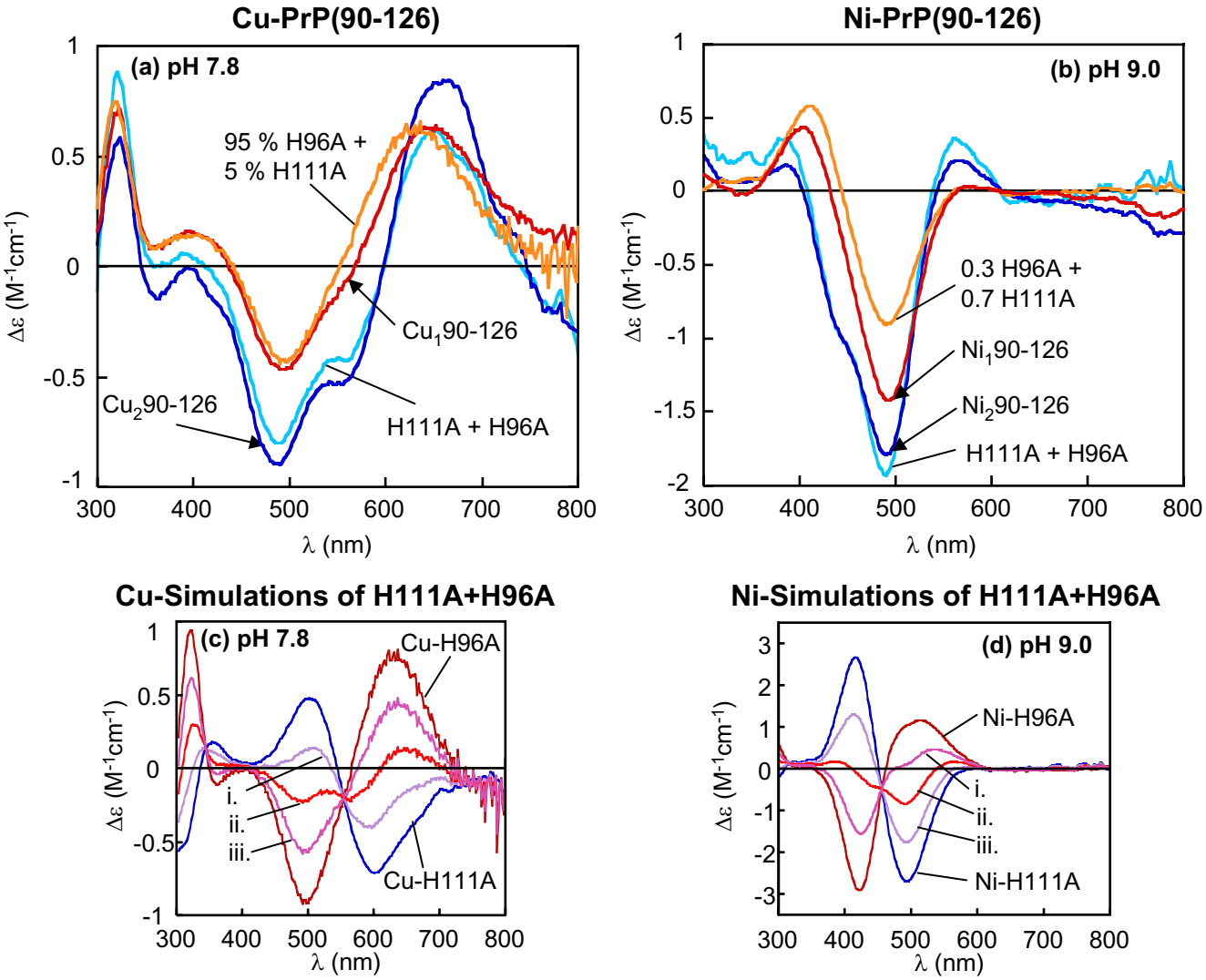

Figure 3. Klewpatinond and Viles

Biochemical Journal Immediate Publication. Published on 2 Mar 2007 as manuscript BJ20061893

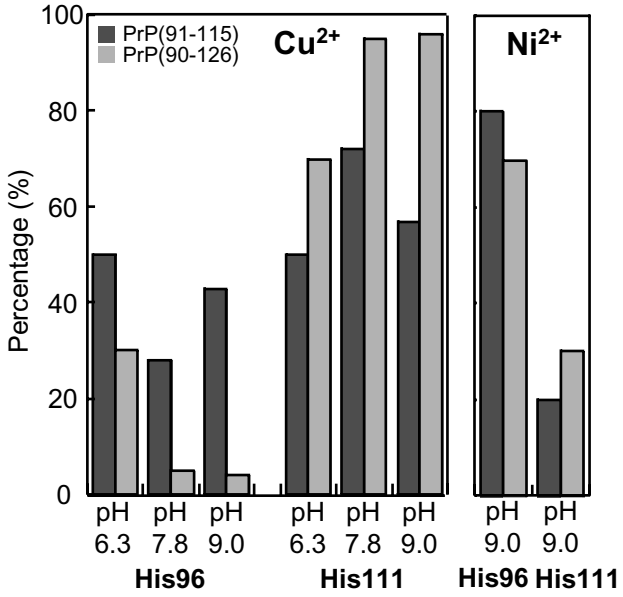

Figure 4. Klewpatinond and Viles

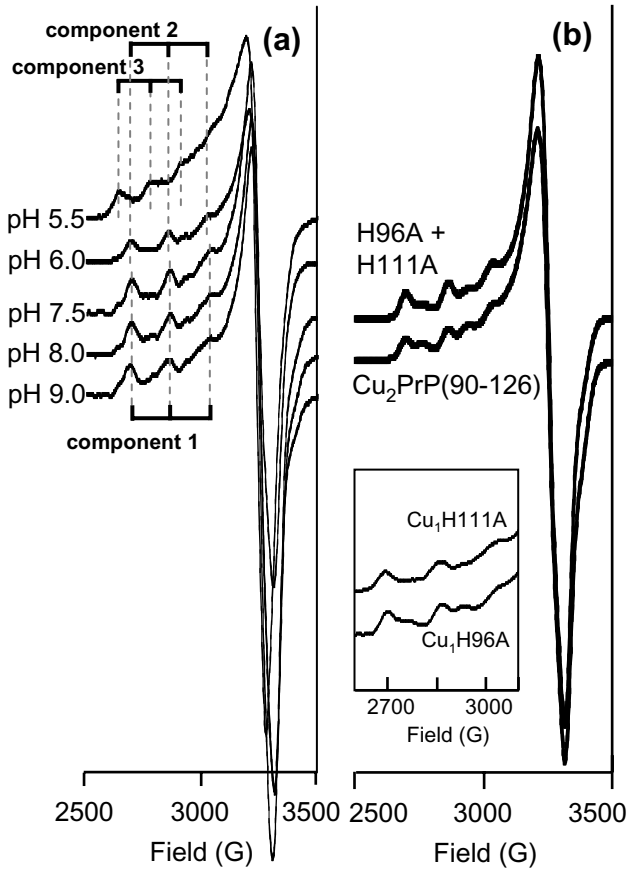

Figure 5. Klewpatinond and Viles

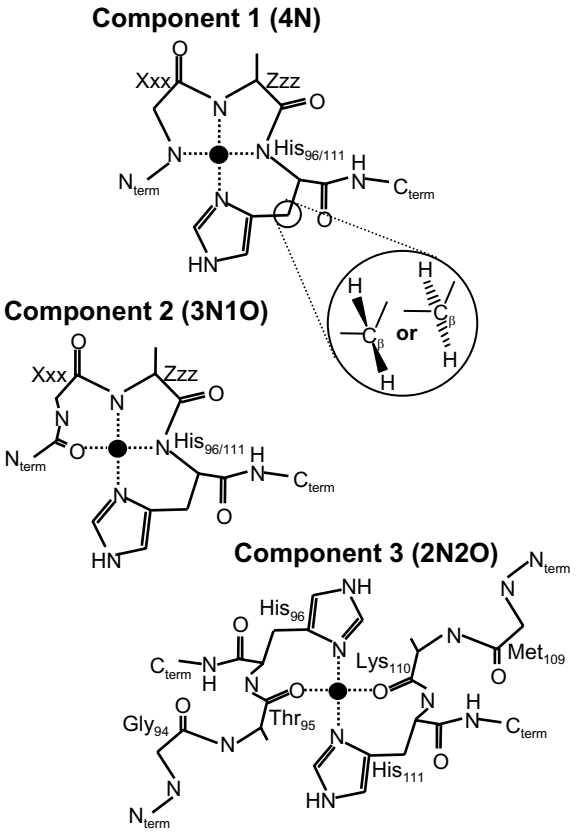

Figure 6. Klewpatinond and Viles

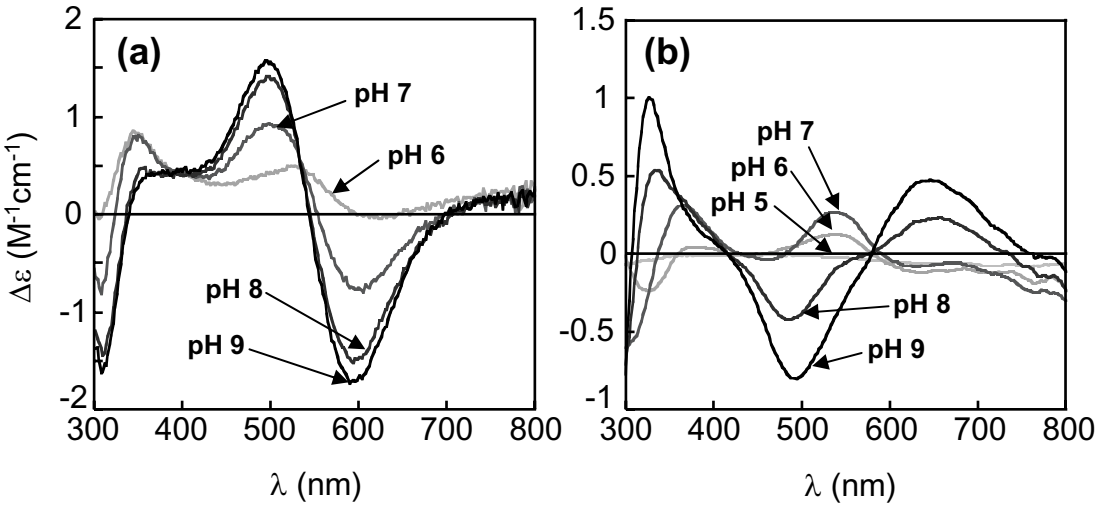

Figure 7. Klewpatinond and Viles

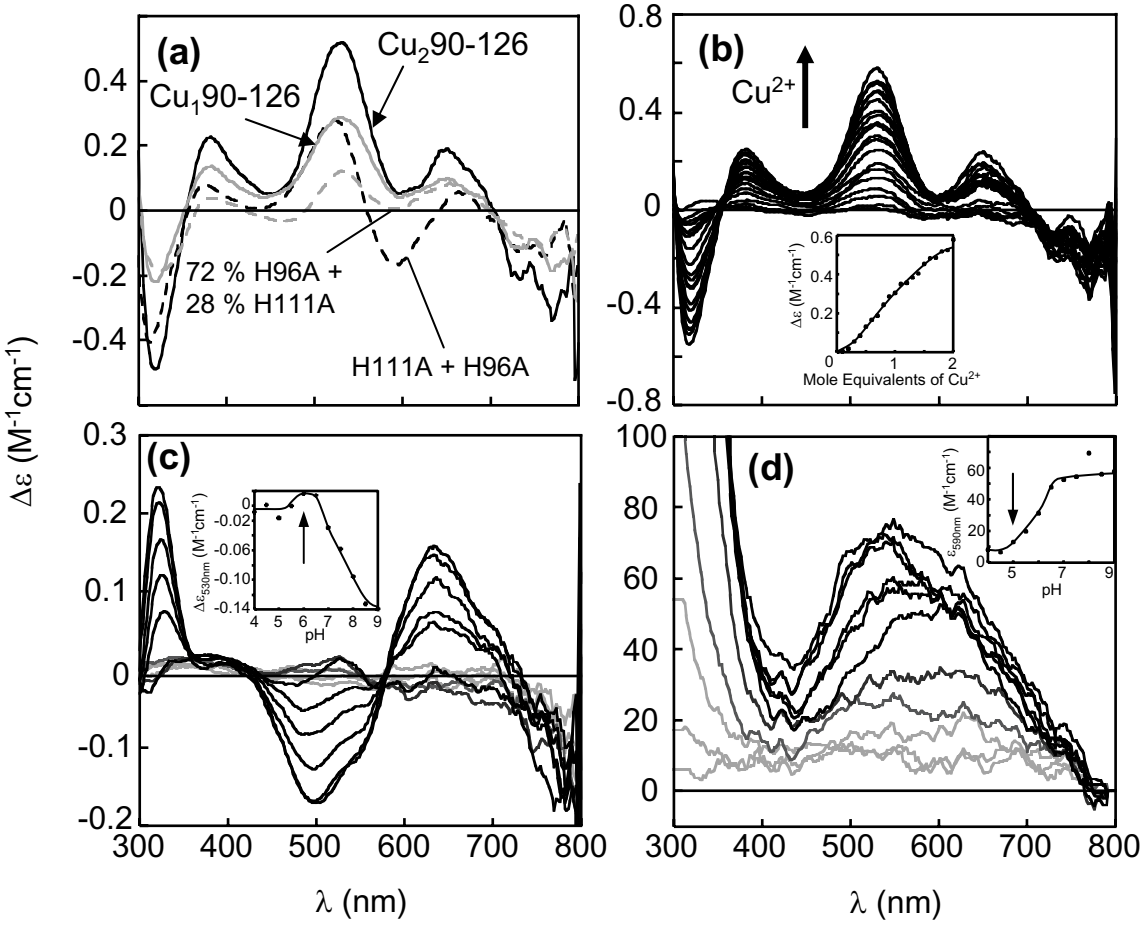

Figure 8. Klewpatinond and Viles

Biochemical Journal Immediate Publication. Published on 2 Mar 2007 as manuscript BJ20061893

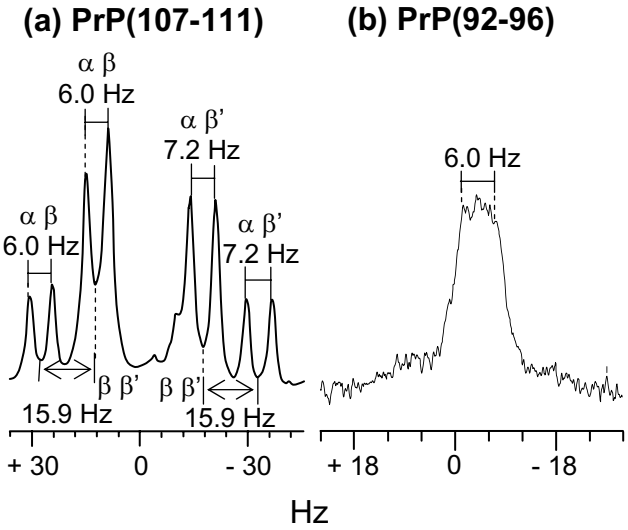

Figure 9. Klewpatinond and Viles